# $Tb^{3+} \rightarrow Ce^{3+}$ energy transfer in $Ce^{3+}$-doped $Y_{3-x}Tb_xGd_{0.65}Al_5O_{12}$



2006 J. Phys.: Condens. Matter 18 10531

(http://iopscience.iop.org/0953-8984/18/47/001)

INSTITUTE OF PHYSICS PUBLISHING JOURNAL OF PHYSICS: CONDENSED MATTER

J. Phys.: Condens. Matter **18** (2006) 10531–10543 doi:10.1088/0953-8984/18/47/001

# $Tb^{3+} \rightarrow Ce^{3+}$ energy transfer in $Ce^{3+}$-doped $Y_{3-x}Tb_xGd_{0.65}Al_5O_{12}$

**R Turos-Matysiak[1], W Gryk[1], M Grinberg[1], Y S Lin[2] and R S Liu[2]**

[1] Institute of Experimental Physics, University of Gdańsk, Wita Stwosza 5, Gdansk, Poland
[2] Department of Chemistry, National Taiwan University, Roosevelt Road, Taipei 106, Taiwan, Republic of China

Received 1 August 2006, in final form 9 September 2006
Published 8 November 2006
Online at stacks.iop.org/JPhysCM/18/10531

**Abstract**

Photoluminescence of $Y_{2.3-x}Tb_xCe_{0.05}Gd_{0.65}Al_5O_{12}$ ($x = 0.575$, 1.15, 1.725 and 2.3) has been measured at room temperature at high hydrostatic pressure. Under excitation at 457 nm, the broad band emission related to interconfigurational transition from the lowest state of excited electronic configurations $5d^1$ to the ground state split by spin–orbit interaction into $^2F_{5/2}$ and $^2F_{7/2}$ components of $Ce^{3+}$ ions, peaked at 550 nm, is seen. Under excitation with 325 nm one observes mainly the sharp luminescence lines related to $^5D_4 \rightarrow {}^7F_6$, $^5D_4 \rightarrow {}^7F_5$, $^5D_4 \rightarrow {}^7F_4$ and $^5D_4 \rightarrow {}^7F_3$ transitions in $Tb^{3+}$ ions. One observes a strong pressure induced red-shift of the $Ce^{3+}$ emission approximately equal to $-20$ cm$^{-1}$ kbar$^{-1}$ and much smaller shifts (approximately $-1$ cm$^{-1}$ kbar$^{-1}$) of the energies of the sharp lines related to $Tb^{3+}$ luminescence. It has been found that the efficiency of $Tb^{3+} \rightarrow Ce^{3+}$ energy transfer depends on Tb content and excitation energy; specifically, it is less effective when $Tb^{3+}$ is excited to the lowest state of the excited $5d^14f^7$ electronic configuration. This effect has been tentatively attributed to the nonradiative de-excitation of the $Tb^{3+}$ ion to the metastable $^5D_4$ state. A configurational model has been developed, which explains peculiarities of relaxation in the excited states of $Tb^{3+}$ and $Tb^{3+} \rightarrow Ce^{3+}$ energy transfer.

## 1. Introduction

$Y_3Al_5O_{12}$ garnet (yttrium aluminium garnet; YAG) has been considered as a host for rare earth doped solid state lasers and phosphors [1]. The last applications concern the phosphors for light emitting diodes (LEDs) based on the InGaN system, which combined with $Ce^{3+}$-doped YAG phosphors can produce white light [2] and have a long operating lifetime up to 100 000 h [3]. A YAG crystal doped with $Ce^{3+}$ yields bright yellow–green luminescence in the region of 500–700 nm, related to the spin and parity allowed $5d^1 \rightarrow 4f^1$ transition in the $Ce^{3+}$ ion. This emission can be excited with high quantum efficiency by two well separated bands peaked at

  

460 and 300 nm related to transition to the states of the $5d^1$ electronic configuration split by the crystal field [4].

It has been found that codoping with $Tb^{3+}$ causes the appearance of a new excitation band of $Ce^{3+}$ emission related $4f^8 \rightarrow 5d^14f^7$ absorption of $Tb^{3+}$ in the YAG:Ce,Tb system [5]. Details of the kinetics of the $Tb^{3+} \rightarrow Ce^{3+}$ energy transfer in YAG have been studied in the framework of the Inokuti–Hirayama model [6] by Liu *et al* [7]. We analyse the $Tb^{3+} \rightarrow Ce^{3+}$ energy transfer processes in mixed garnet powders of composition $Y_{2.3-x}Tb_xCe_{0.05}Gd_{0.65}$ ($x = 0.575$, 1.15, 1.725 and 2.3). Basic spectroscopy of these materials has been reported in paper [2]. In this paper, the photoluminescence, photoluminescence excitation spectra and photoluminescence spectra obtained under various excitations at high hydrostatic pressure will be reported. High hydrostatic pressure as well as the crystal content influences the energy of excited states belonging to the $5d^1$ electronic configuration of $Ce^{3+}$ and to the $5d^14f^7$ electronic configuration of $Tb^{3+}$, the energies of the states of the ground electronic configurations remaining almost unchanged. Thus applying pressure one can control the energy resonance between the donor ($Tb^{3+}$) and acceptor ($Ce^{3+}$). The main purpose of our study is the analysis of the relaxation process in the excited states of $Tb^{3+}$ and finding the actual state which is the initial one in the $Tb^{3+} \rightarrow Ce^{3+}$ energy transfer process.

## 2. Experimental details

The mixed garnet crystals $(Y_{2.3-y}Ce_{0.05}Gd_y)Al_5O_{12}$ and $(Y_{2.3-x-y}Tb_xCe_{0.05}Gd_y)Al_5O_{12}$ in the powdered form were synthesized by a three step solid state reaction from a mixture of metal nitrides and metal oxides at temperature below 1600 °C. Details of sample preparation are described in [2]. We have at our disposal five samples with Gd and Tb content given by $y = 0.65$, the same for all samples, and $x = 0$, 0.575, 1.15, 1.725 and 2.3.

Luminescence excitation has been measured using a home made system consisting of an Xe lamp (1000 W), two monochromators type SPM2 (one for excitation and one for detection) and two photomultipliers (the first for the luminescence detection and the second for a reference signal). To obtain the $Ce^{3+}$ luminescence we have excited the system with an Ar laser with wavelength 457 nm, whereas to obtain the $Tb^{3+}$ luminescence we have excited the system with an He–Cd laser with wavelength 325 nm. Pressure up to 150 kbar has been applied using a diamond anvil cell (DAC). Dimethylsiloxane oil has been used as the pressure transmitting medium and a ruby ($Al_2O_3$:$Cr^{3+}$) crystal has been used as the pressure sensor. The emission under high pressure has been dispersed with a PGS 2 spectrometer working as a monochromator and collected by an R943-02 Hamamatsu photomultiplier working in the photon counting regime. All spectra have been corrected with respect to the apparatus response. The luminescence intensities were adjusted by the factor $\nu^{-3}$, where $\nu$ is the emission frequency. The reason for the adjustment is that for broad band luminescence consisting of a number of vibronic components the radiative rates of those emitting at higher frequency are enhanced by the energy-dependent photon density of states [8].

## 3. Spectroscopy of $Ce^{3+}$ ions

### *3.1. Luminescence and luminescence excitation spectra*

Luminescence spectra under excitation with wavelength 457 nm and excitation spectra of luminescence monitored at 560 nm (corresponding to the maximum of the $Ce^{3+}$ emission) of the $(Y_{2.3-x}Tb_xCe_{0.05}Gd_{0.65})Al_5O_{12}$ systems are presented in figure 1(a). We have presented the emission only for $x = 0$, 0.575 and 2.3. The luminescence lineshapes for $x = 1.15$ and 1.725 look very similar. One can see that for all materials the emission consists of the broad band

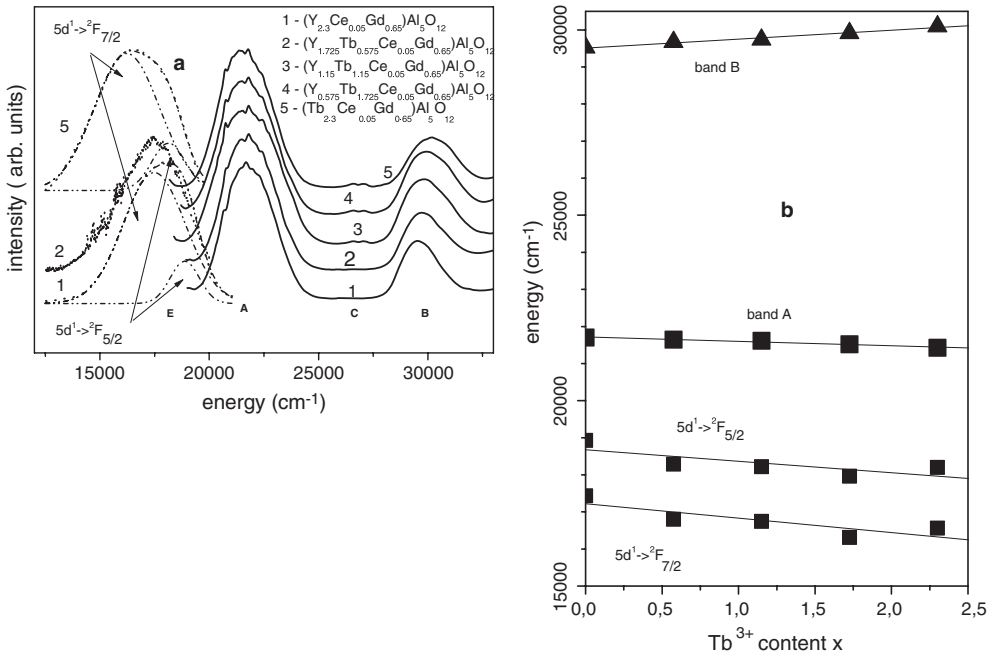


**Figure 1.** (a) Luminescence excitation spectra of the $(Y_{2.3-x}Tb_xCe_{0.05}Gd_{0.65})Al_5O_{12}$ containing different $Tb^{3+}$ contents, '$x$'. Luminescence has been monitored at 560 nm, which corresponds to the maximum of the $Ce^{3+}$ luminescence. Curves 1, 2, 3, 4 and 5 correspond to terbium content $x = 0$, 0.575, 1.15, 1.725 and 2.3, respectively. On the left side of the figure the emission spectra are presented (labelled by E). Gaussian bands corresponding to the $5d^1 \rightarrow {}^2F_{5/2}$ and $5d^1 \rightarrow {}^2F_{7/2}$ transitions are presented by dashed–dotted curves. (b) Luminescence excitation spectrum peak positions and $Ce^{3+}$ luminescence peak positions versus Tb content.

luminescence related to the internal $5d^1 \rightarrow 4f^1$ ($^2F_{5/2}$, $^2F_{7/2}$) transition in $Ce^{3+}$ ions. Adjusted luminescence spectra can then be fitted to two Gaussians corresponding to the transitions to the $^2F_{5/2}$ and $^2F_{7/2}$ components of the $Ce^{3+}$ ground state. These bands are presented in figure 1(a) by dashed–dotted curves. Energies of the maxima of the $5d^1 \rightarrow {}^2F_{5/2}$, $^2F_{7/2}$ transitions versus $Tb^{3+}$ concentration are presented in figure 1(b).

In the range of 33 300 $cm^{-1}$ (300 nm) to 19 500 $cm^{-1}$ (525 nm) the luminescence excitation spectra consist of two broad bands peaked at 21 720 $cm^{-1}$ (band A) and at 29 510 $cm^{-1}$ (band B) and correspond to optical transitions from the ground state of $Ce^{3+}$ to crystal field split states of excited electronic configuration $5d^1$ [4, 9]. For samples containing terbium, additional structure with peaks at 26 576 and 27 060 $cm^{-1}$ appears and is related to the $^7F_6 \rightarrow {}^5D_5$ transition in the $Tb^{3+}$ ion, labelled by C in figure 1. One notices the strong shift of the A band towards lower energy and B band towards higher energy versus $Tb^{3+}$ concentration. The positions of maxima of A and B for different Tb content '$x$' are presented in figure 1(b). The rates defined as $\frac{dE}{dx}$ are equal to $-120 \pm 13$ and $240 \pm 21$ $cm^{-1}$ for A and B bands, respectively. The dependence of the energies of bands A and B on Tb content can be related to the increase of the crystal field in the $Ce^{3+}$ site.

It has been shown that the lattice constant of $(Y_{2.3-x}Tb_xCe_{0.05}Gd_{0.65})Al_5O_{12}$ increases almost linearly with terbium concentration from 12.03 Å for $x = 0$ to 12.09 Å for $x = 2.3$ [2]. The increase of lattice constant is a result of difference in ionic radii, which for $Tb^{3+}$ is equal to 1.04 Å and for $Y^{3+}$ is equal to 1.019 Å (the $Ce^{3+}$ ionic radius is equal to 1.143 Å) [10]. It is

**Table 1.** Energies of the d–f luminescence in $Ce^{3+}$ ions.

| | $5d^1 \rightarrow {}^2F_{5/2}$ | | $5d^1 \rightarrow {}^2F_{7/2}$ | |
|---|---|---|---|---|
| Material | Energy ($cm^{-1}$) | Pressure shift ($cm^{-1}$ $kbar^{-1}$) | Energy ($cm^{-1}$) | Pressure shift ($cm^{-1}$ $kbar^{-1}$) |
| $(Y_{2.3}Ce_{0.05}Gd_{0.65})Al_5O_{12}$ | $17\,435 \pm 100$ | $-20 \pm 2$ | $18\,926 \pm 100$ | $-23 \pm 2$ |
| $(Y_{1.725}Tb_{0.575}Ce_{0.05}Gd_{0.65})Al_5O_{12}$ | $16\,803 \pm 130$ | $-17 \pm 3$ | $18\,287 \pm 100$ | $-17 \pm 2$ |
| $(Y_{1.15}Tb_{1.15}Ce_{0.05}Gd_{0.65})Al_5O_{12}$ | $16\,743 \pm 200$ | $-17 \pm 5$ | $18\,228 \pm 200$ | $-17 \pm 4$ |
| $(Y_{0.575}Tb_{1.725}Ce_{0.05}Gd_{0.65})Al_5O_{12}$ | $16\,310 \pm 200$ | $-17 \pm 4$ | $17\,960 \pm 200$ | $-16 \pm 2$ |
| $(Tb_{2.3}Ce_{0.05}Gd_{0.65})Al_5O_{12}$ | $16\,565 \pm 200$ | $-18 \pm 3$ | $18\,200 \pm 200$ | $-16 \pm 2$ |

expected that an increase of lattice constant would be accompanied by a decrease of the crystal field in the $Ce^{3+}$ site. The opposite effect of increase of crystal field is surprising, and can be attributed to local compression of the $CeO_8$ complex when smaller $Y^{3+}$ ions are replaced by larger $Tb^{3+}$ ions. Actually, $Tb^{3+}$ has to expand the lattice locally only in the sites where it replaces $Y^{3+}$ ions. There is no reason why the $Ce^{3+}$–$O^{2-}$ bond length should increase as a response to the $Tb^{3+}$ incorporation. The more natural effect is local compression of the $CeO_8$ complex as the lattice response on expansion of $TbO_8$ sites.

### *3.2. Pressure dependence of the $Ce^{3+}$ emission spectra*

High pressure emission spectra of $(Y_{2.3-x}Tb_xCe_{0.05}Gd_{0.65})Al_5O_{12}$ for $x = 0$, 0.575 and 2.3 obtained under excitation of 457 nm are presented in figures 2(a)–(c), respectively. High pressure emission of the materials with $Tb^{3+}$ content $x = 1.15$ and 1.725 under this excitation also consists only of $Ce^{3+}$ luminescence and looks very similar to these presented in figures 2(a)–(c). Similarly to the case of ambient pressure, the emission band can be decomposed into two Gaussian bands corresponding to the $5d^1 \rightarrow {}^2F_{5/2}$, ${}^2F_{7/2}$ transitions. An evident red-shift of the emission (of both bands) with pressure has been observed for all materials. The maximum positions of fitted bands for all materials versus pressure are presented in figure 3. The best linear fits of their dependences on pressure are presented by solid lines. The fitted energies of the maxima of the Gaussian bands and their pressure shifts are additionally presented in table 1. The pressure shifts of individual bands are slightly different in different samples. Specifically, the pressure shifts are slightly larger in $(Y_{2.3}Ce_{0.05}Gd_{0.65})Al_5O_{12}$ than in $(Tb_{2.3}Ce_{0.05}Gd_{0.65})Al_5O_{12}$ and mixed crystals; nevertheless, due to large statistical error one cannot discuss any systematic trends in detail. Generally in our samples the shifts are greater than the quantity $-12.5 \pm 1$ $cm^{-1}$ $kbar^{-1}$ obtained previously for a bulk YAG:$Ce^{3+}$ crystal [11]. The increase of emission pressure shift can be related to the diminishing of compressibility caused by incorporation of $Gd^{3+}$ into the YAG crystal. One notices that $Tb^{3+}$ content hardly influences the pressure shifts. One notices that energies of the $5d^1 \rightarrow {}^2F_{5/2}$ and $5d^1 \rightarrow {}^2F_{7/2}$ transitions also depend on Tb content. The position of respective peaks versus $x$ are presented in figure 1(b). Changes are almost linear and the rates defined as $\frac{dE}{dx}$ are equal to $-300 \pm 150$ $cm^{-1}$ and $-400 \pm 150$ $cm^{-1}$ for the $5d^1 \rightarrow {}^2F_{5/2}$ and $5d^1 \rightarrow {}^2F_{7/2}$ transition, respectively.

### *3.3. Configurational model of the $Ce^{3+}$ system*

A configurational coordinate diagram describing the energetic structure of the $Ce^{3+}$ is presented in figure 4(a). The two lowest parabolas represent the ground electronic configuration $4f^1$ split

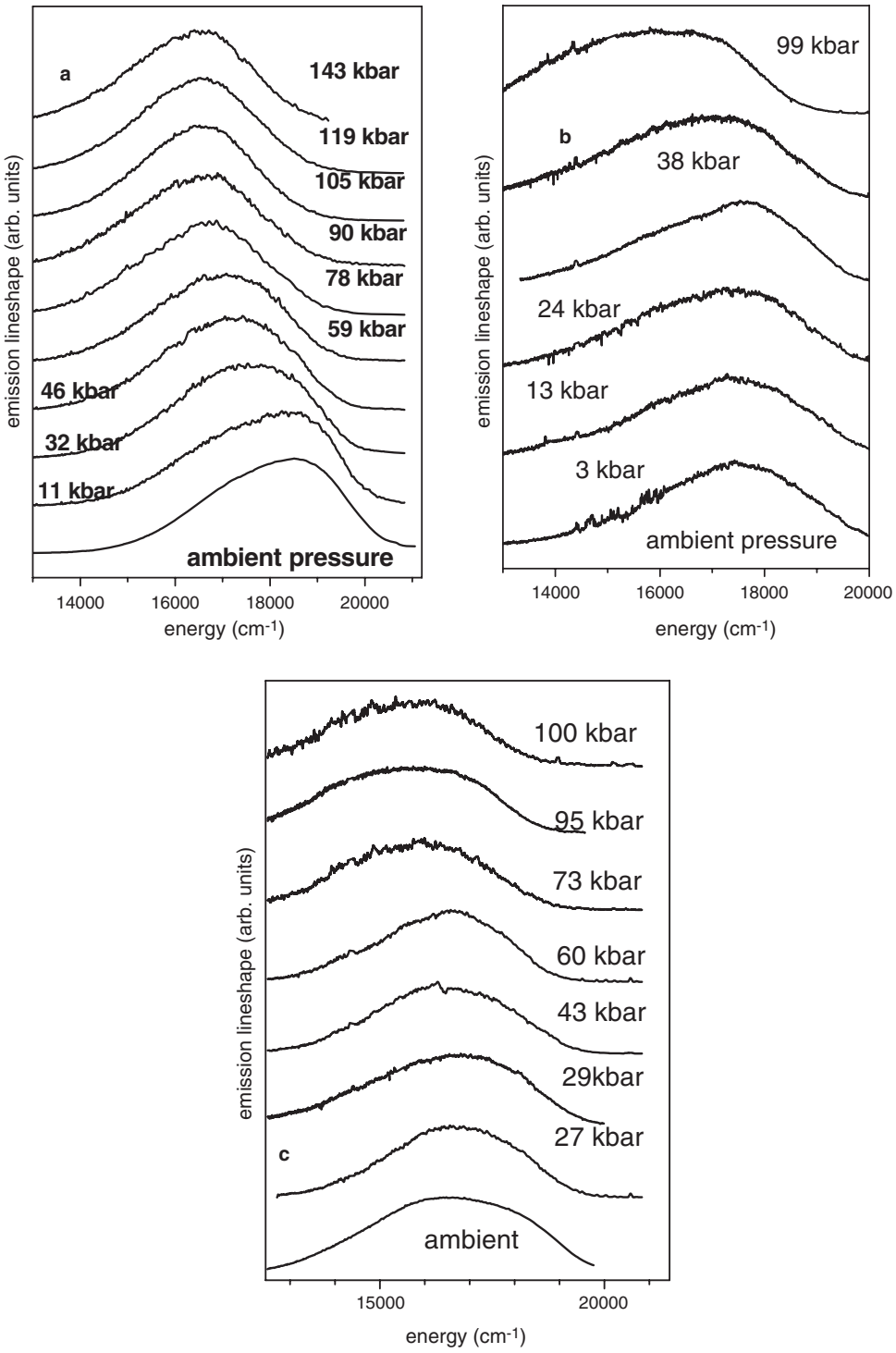


**Figure 2.** Luminescence spectra obtained under selected pressures. The spectra of $(Y_{2.3}Ce_{0.05}Gd_{0.65})Al_5O_{12}$, $(Y_{1.725}Tb_{0.575}Ce_{0.05}Gd_{0.65})Al_5O_{12}$ and $(Tb_{2.3}Ce_{0.05}Gd_{0.65})Al_5O_{12}$ are presented in (a)–(c), respectively.

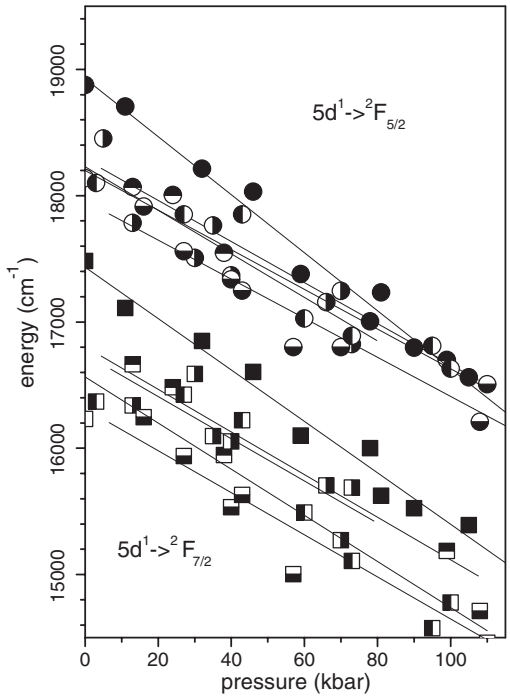


**Figure 3.** Positions of the emission peaks related to the $5d^1 \rightarrow {}^2F_{5/2}$ and $5d^1 \rightarrow {}^2F_{7/2}$ luminescence of $Ce^{3+}$. Experimental data are represented by circles and rectangles, for $5d^1 \rightarrow {}^2F_{5/2}$ and $5d^1 \rightarrow {}^2F_{7/2}$ transitions, respectively. Symbols ●■, ◓⬒, ◑◨, ◒⬓ and ◐◧ correspond to terbium content $x = 0$, 0.575, 1.15, 1.725 and 2.3, respectively; solid lines correspond to the linear fits.

by spin–orbit interaction into ${}^2F_{5/2}$ (the ground state) and ${}^2F_{7/2}$ (the first excited state). The lowest states of excited electronic configuration $5d^1$ are represented by two higher parabolas. These states are labelled by irreducible representations of the $O_h$ point group ${}^2E$ (fourfold degeneration) and ${}^2T_2$ (sixfold degeneration). The energy of the ${}^2E$–${}^2T_2$ splitting $\Delta$ depends on Tb concentration, $x$, and is given by the relation $\Delta = [7800 + 360 * x]\ \mathrm{cm}^{-1}$. Compression of the $CeO_8$ complex caused by pressure resulted in additional increasing of the splitting energy $\Delta$ and diminishing energy of the ${}^2E$ state. This effect produces a pressure red-shift of the $Ce^{3+}$ emission.

Electron–lattice interaction in the excited electronic manifold causes the shift of the respective parabolas in the configurational space. One describes electron–lattice interaction using the quantity $S\hbar\omega$ ($S$ is the Huang–Rhys factor and $\hbar\omega$ is the energy of the local phonon mode) defined as the lattice relaxation energy in the excited state. Considering the lattice relaxation energy as half of the Stokes shift (the difference between maxima of luminescence excitation and emission spectra), one has obtained $S\hbar\omega = 1530\ \mathrm{cm}^{-1}$ for the $(Y_{2.3}Ce_{0.05}Gd_{0.65})Al_5O_{12}$ crystal. An evident increase of this energy with concentration of $Tb^{3+}$ has been observed: $\frac{\mathrm{d}S\hbar\omega}{\mathrm{d}x} = 140\ \mathrm{cm}^{-1}$.

Let us focus on the dependence of the $Ce^{3+}$ absorption bands (see the luminescence excitation spectra in figure 1(a)) on Tb concentration. According to the crystal field model the dependence of the energies of the ${}^2E$ and ${}^2T_2$ states of the $5d^1$ electronic configuration in dodecahedral coordination on crystal field strength $10Dq$ can be expressed in the same way as

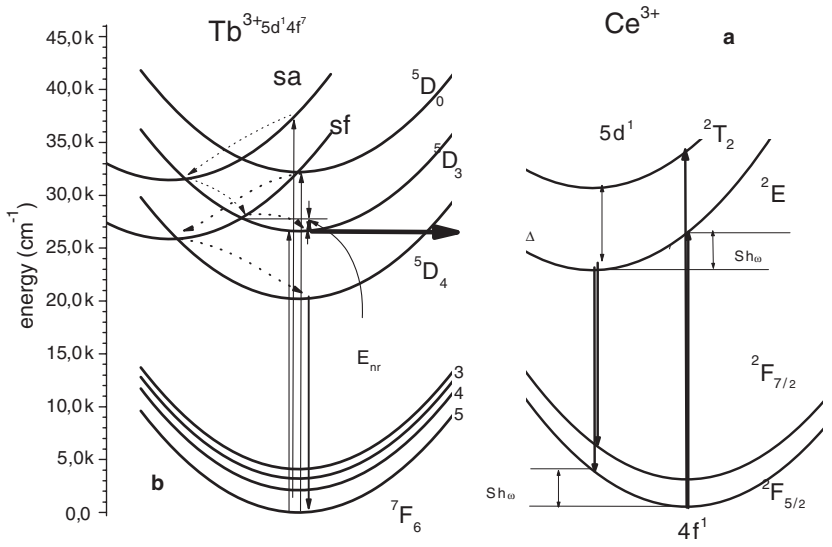


**Figure 4.** Configurational coordinate diagrams of the $Ce^{3+}$ (a) and $Tb^{3+}$ (b) systems. The dotted arrows represent the possible nonradiative de-excitation processes that cause $Tb^{3+}$ luminescence, the solid horizontal arrow represents the possible process that causes the $Tb^{3+}$ to $Ce^{3+}$ energy transfer and the solid vertical arrows represent the radiative transitions. The excited states labelled as 'sa' and 'sf' in (b) represent the states of the $5d^14f^7$ electronic configuration of multiplicity $2S+1$ equal to 7 and 5, respectively.

for the respective states of the $3d^1$ electronic configuration [11, 12]. One obtains

$$\begin{aligned} E_{^2T_2} &= E^0_{5d} + \tfrac{32}{9}Dq \\ E_{^2E} &= E^0_{5d} - \tfrac{32}{6}Dq \end{aligned} \tag{1}$$

where $E^0_{5d}$ is the energy of the barycentre of the $5d^1$ electronic configuration. Under the assumption that $E^0_{5d}$ does not depend on $x$, relations (1) yield that the absolute shift of the energy of the $^2E$ state should be equal to about 3/2 of the respective shift of the $^2T_2$ state. Our experimental data yield the opposite result, $\frac{dE_{^2E}}{dx} = -120 \pm 13$ cm$^{-1}$ and $\frac{dE_{^2T_2}}{dx} = 240 \pm 21$ cm$^{-1}$. Thus the increase of crystal field is not the only reason for the changes of energies of the $^2E$ and $^2T_2$ states. If one assumes that the crystal field model works, the additional effect of the increase of $x$ is the increase of energies of all states of the $5d^1$ electronic configuration with respect to the states of the $4f^1$ electronic configuration, defined as $\frac{dE^0_{5d}}{dx}$. Relations (1) allow us to obtain

$$\begin{aligned} \frac{dE_{^2T_2}}{dx} &= \frac{dE^0_{5d}}{dx} + \frac{32}{9}\frac{dDq}{dx} \\ \frac{dE_{^2E}}{dx} &= \frac{dE^0_{5d}}{dx} - \frac{32}{6}\frac{dDq}{dx} \end{aligned} \tag{2}$$

and yield the barycentre energy shift $\frac{dE^0_{5d}}{dx} = 96$ cm$^{-1}$.

The effect can be attributed to diminishing of the centroid shift related to changes in ligand polarization accompanying the transition of an electron from the f to the d shell [13].

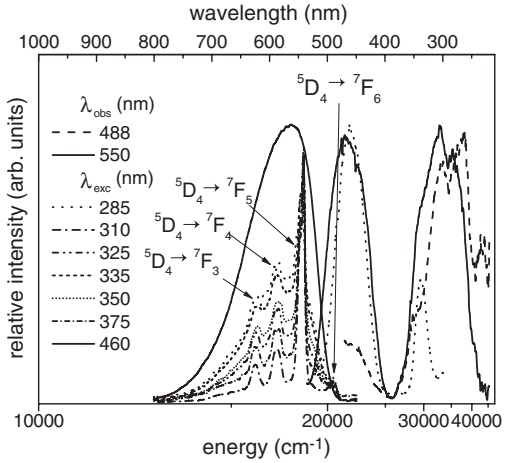


**Figure 5.** Luminescence of $(Y_{1.725}Tb_{0.575}Ce_{0.05}Gd_{0.65})Al_5O_{12}$ under various excitations (right side of the figure, see the labelling in the figure). On the left side of the figure the luminescence excitation spectra are presented by dashed and solid curves, for luminescence monitored at 488 and 550 nm, respectively. The $Ce^{3+}$ excitation spectra (for emission monitored at 560 nm) is represented by a dotted curve.

## 4. Spectroscopy of $Tb^{3+}$ ion

### *4.1. Luminescence and luminescence excitation spectra*

In figure 5 luminescence spectra of the $(Y_{1.725}Tb_{0.575}Ce_{0.05}Gd_{0.65})Al_5O_{12}$ under different excitations are presented. The spectrum is a superposition of a broad band related to $Ce^{3+}$ and sharp lines related to $Tb^{3+}$. We have observed the lines related to $^5D_4 \rightarrow {}^7F_6$, $^5D_4 \rightarrow {}^7F_5$, $^5D_4 \rightarrow {}^7F_4$ and $^5D_4 \rightarrow {}^7F_3$ transitions (see the respective peaks in figure 5). We have measured the excitation spectrum of luminescence monitored at 550 nm, corresponding partly to $Ce^{3+}$ emission and partly to $^5D_4 \rightarrow {}^7F_5$ emission of $Tb^{3+}$, and 488 nm, that is related mainly to $^5D_4 \rightarrow {}^7F_6$ emission of $Tb^{3+}$. In the former case the excitation spectrum consists of the broad band peaked at 450 nm, which is related to the lower f–d transition in $Ce^{3+}$ (band A in figure 1) and a more structured band peaked at about 300 nm related to f–d transitions in $Tb^{3+}$. It is known that energies 36 450 $cm^{-1}$ (274 nm) and 30 864 $cm^{-1}$ (324 nm) correspond to the spin allowed and spin forbidden $4f^8 \rightarrow 5d^14f^7$ transition in the $Tb^{3+}$ ion, respectively [14]. The relation of the excitation band at 300 nm to absorption of $Tb^{3+}$ is demonstrated when the excitation spectrum of the emission monitored at 488 nm is measured. Actually, the $^5D_4 \rightarrow {}^7F_6$ luminescence is effectively excited by a double band with maxima at 320 and 270 nm. Comparing the excitation spectra for luminescence monitored at 560, 488 and 550 nm one notices that the excitation spectrum of emission 550 nm (solid curve) can be considered as a superposition of two others: the excitation spectrum of $Tb^{3+}$ luminescence monitored at 488 nm (dashed curve) and $Ce^{3+}$ luminescence monitored at 560 nm (dotted curve). This is expected since the luminescence at 550 nm is a superposition of $Tb^{3+}$ and $Ce^{3+}$ emission.

A similar effect of appearance of $Tb^{3+}$ emission under specific excitation has been observed for all powders containing terbium. Specifically, under excitation with an He–Cd laser with wavelength 325 nm in all samples sharp luminescence lines related to $Tb^{3+}$ have been dominant.

### *4.2. Pressure dependence of the $Tb^{3+}$ luminescence spectra*

Emission spectra under excitation 325 nm obtained for different pressures for the $(Y_{2.3-x}Tb_xCe_{0.05}Gd_{0.65})Al_5O_{12}$ for $x = 0$, 0.575, 1.725 and 2.3 are presented in figures 6(a)–(c), respectively. The dominant luminescence consists of the sharp lines related to the $^5D_4 \rightarrow {}^7F_6$, $^5D_4 \rightarrow {}^7F_5$, $^5D_4 \rightarrow {}^7F_4$ and $^5D_4 \rightarrow {}^7F_3$ transitions in the $Tb^{3+}$ ions. One notices the small red-shifts of the energies of the transitions with pressure. Ambient pressure energies of these lines and the respective pressure shifts are listed in table 2. The shifts are the largest for $(Y_{1.725}Tb_{0.575}Ce_{0.05}Gd_{0.65})Al_5O_{12}$. Pressure changes of the f–f luminescence are small and are related to pressure induced reduction of the quantities of Slater integrals and spin–orbit coupling parameter [15, 16]. All spectra presented in figures 6(a)–(c) contain a trace of the broad band emission of $Ce^{3+}$, peaked at about 17 500 $cm^{-1}$ and characterized by a large red pressure shift. One notices that the relative intensity of this band with respect to the sharp $Tb^{3+}$ emission lines seems to be pressure independent.

## 5. Configurational model of the $Tb^{3+}$ system and $Tb^{3+} \rightarrow Ce^{3+}$ energy transfer

The energetic structure and radiative and nonradiative processes in $Tb^{3+}$ are presented in a configurational coordinate diagram in figure 4(b). In the figure the $^7F_J$ states of the ground multiplet and the $^5D_0$, $^5D_3$ and $^5D_4$ states of the $4f^8$ electronic configuration, and two states belonging to the $5d^14f^7$ electronic configuration, are presented. The parabolas of the $5d^14f^7$ electronic configuration labelled as 'sa' and 'sf' represent the states of multiplicity $2S + 1$ equal to seven and nine, respectively. These parabolas are shifted in the configurational space due to electron–lattice coupling. Under excitation through $4f^8 \rightarrow 5d^14f^7$ transitions in the $Tb^{3+}$ ion at 230–330 nm the system can relax nonradiatively to the $^5D_4$ state and then yield $Tb^{3+}$ emission. The respective de-excitation pathways are indicated in figure 4(b) by dashed arrows.

Considering the spectra presented in figure 5 one notices that after excitation with wavelength 310 and 375 nm corresponding to the direct excitation to the $^5D_3$ and $^5D_0$ states of the $Tb^{3+}$ ion the emission spectrum is dominated by $Tb^{3+}$ luminescence. Under excitation with other wavelengths (specifically with 285 nm, that corresponds to the region of the spin allowed $4f^8 \rightarrow 5d^14f^7$ transition in the $Tb^{3+}$ ion) one obtains both $Tb^{3+}$ and $Ce^{3+}$ emission, but $Ce^{3+}$ emission dominates. One notices the following.

(i) $Tb^{3+}$ luminescence is obtained in all Tb containing samples under excitation 310–325 nm.
(ii) In $(Y_{1.725}Tb_{0.575}Ce_{0.05}Gd_{0.65})Al_5O_{12}$ intensive $Tb^{3+}$ emission is also observed for other excitations between 200 and 375 nm (see figure 5), whereas in samples with larger concentration of Tb $Tb^{3+}$ emission under this excitation does not exist or is much less effective.

Thus effective energy transfer from $Tb^{3+}$ to $Ce^{3+}$ can take place when both ions are close to each other and we have a large concentration of $Tb^{3+}$ that allows the effective energy transfer between $Tb^{3+}$ ions and between $Tb^{3+}$ and $Ce^{3+}$ ions. Actually, only for $x = 0.575$ does the $Tb^{3+}$ emission exist for excitation other than 325 nm. This may be because in the material with the lowest Tb concentration some of the $Tb^{3+}$ ions are too far from other $Tb^{3+}$ and $Ce^{3+}$ and therefore emit light as individual impurities.

One can consider the possible mechanism of energy transfer using diagrams presented in figures 4(a) and (b). As has been mentioned, under excitations 26 670 $cm^{-1}$ (375 nm) and 32 250–30 770 $cm^{-1}$ (310–325 nm) that correspond to direct excitation to the $^5D_3$ and $^5D_0$ states of the $Tb^{3+}$ ion, respectively, we observe more intense $Tb^{3+}$ luminescence, whereas

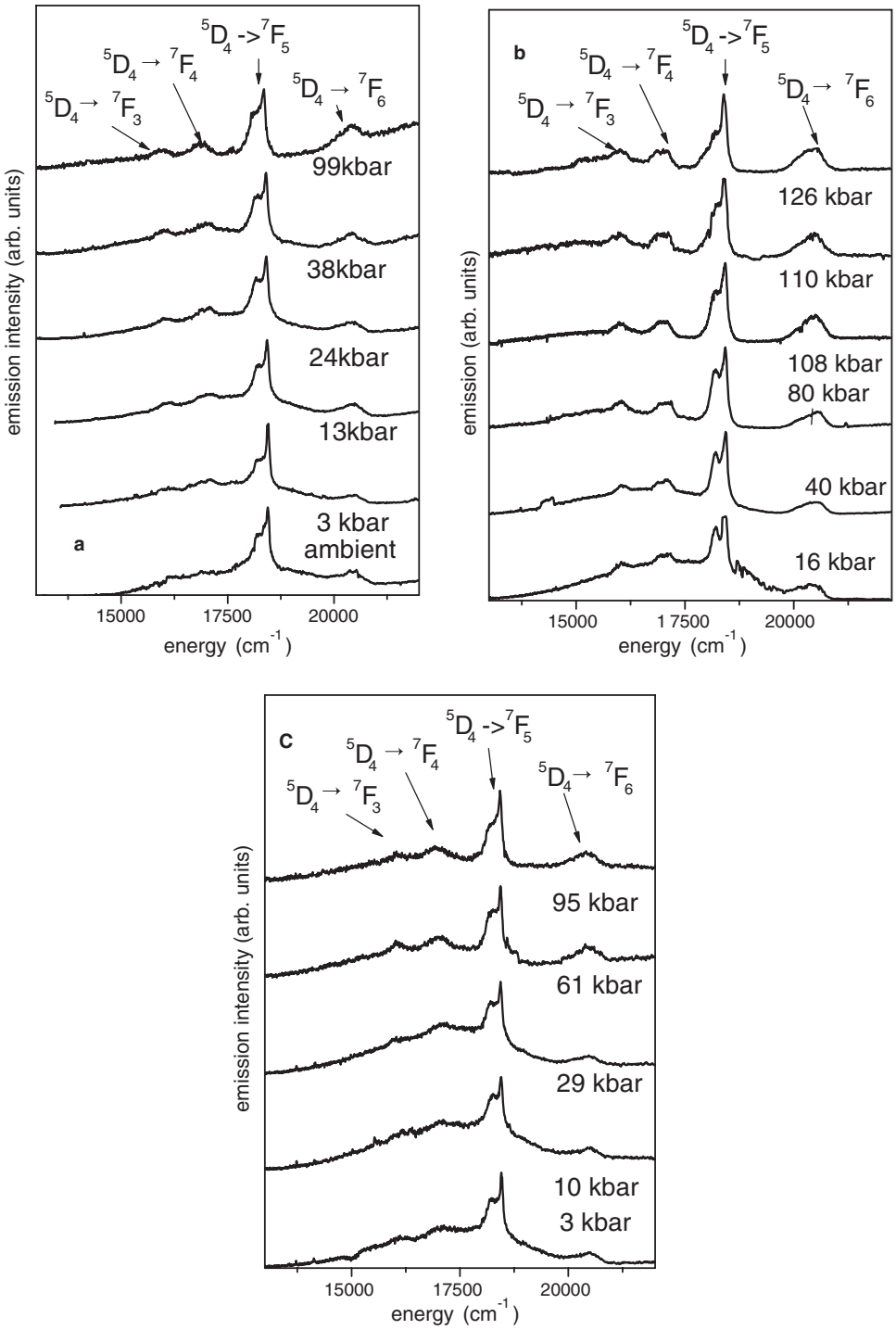


**Figure 6.** Luminescence under excitation 325 nm obtained for selected pressures for $(Y_{1.725}Tb_{0.575}Ce_{0.05}Gd_{0.65})Al_5O_{12}$ (a), for $(Y_{0.575}Tb_{1.725}Ce_{0.05}Gd_{0.65})Al_5O_{12}$ (b) and for $(Tb_{2.5}Ce_{0.05}Gd_{0.65})Al_5O_{12}$ (c).

**Table 2.** Energies of the f–f luminescence in $Tb^{3+}$ ions.

| | $^5D_4 \rightarrow {}^7F_6$ | | $^5D_4 \rightarrow {}^7F_5$ | | $^5D_4 \rightarrow {}^7F_4$ | | $^5D_4 \rightarrow {}^7F_3$ | |
|---|---|---|---|---|---|---|---|---|
| Material | Energy ($cm^{-1}$) | Pressure shift ($cm^{-1}$ $kbar^{-1}$) | Energy ($cm^{-1}$) | Pressure shift ($cm^{-1}$ $kbar^{-1}$) | Energy ($cm^{-1}$) | Pressure shift ($cm^{-1}$ $kbar^{-1}$) | Energy ($cm^{-1}$) | Pressure shift ($cm^{-1}$ $kbar^{-1}$) |
| $(Y_{1.725}Tb_{0.575}Ce_{0.05}Gd_{0.65})Al_5O_{12}$ | $20\,405 \pm 10$ | $0.1 \pm 0.2$ | $18\,442 \pm 4$ | $-1.0 \pm 0.1$ | $17\,056 \pm 8$ | $-1.8 \pm 0.2$ | $16\,069 \pm 15$ | $-1.1 \pm 0.2$ |
| | | | $18\,227 \pm 20$ | $-1.3 \pm 0.2$ | | | | |
| $(Y_{1.15}Tb_{1.15}Ce_{0.05}Gd_{0.65})Al_5O_{12}$ | | | $18\,436 \pm 6$ | $-0.3 \pm 0.1$ | | | | |
| | | | $18\,254 \pm 11$ | $0.1 \pm 0.2$ | | | | |
| $(Y_{0.575}Tb_{1.725}Ce_{0.05}Gd_{0.65})Al_5O_{12}$ | $20\,396 \pm 20$ | $0.13 \pm 0.22$ | $18\,410 \pm 3$ | $-0.14 \pm 0.02$ | $17\,045 \pm 23$ | $-0.61 \pm 0.3$ | $16\,100 \pm 15$ | $-0.84 \pm 0.2$ |
| | | | $18\,226 \pm 20$ | $-0.03 \pm 0.02$ | | | | |
| $(Tb_{2.3}Ce_{0.05}Gd_{0.65})Al_5O_{12}$ | $20\,484 \pm 15$ | $-0.6 \pm 0.1$ | $18\,451 \pm 4$ | $-0.28 \pm 0.1$ | $17\,104 \pm 10$ | $-1.0 \pm 0.2$ | $16\,075 \pm 30$ | $0.0 \pm 0.5$ |
| | | | $18\,219 \pm 20$ | $-0.11 \pm 0.1$ | | | | |

for excitation with other wavelengths in the region of the 230–380 nm band the $Ce^{3+}$ luminescence dominates. This general effect results from the fact that the $4f^8 \rightarrow 5d^1 4f^7$ excitation band of $Tb^{3+}$ overlaps energetically with the $4f^1 \rightarrow 5d^1$ excitation band (B band) of $Ce^{3+}$.

For analysis of $Tb^{3+}$ to $Ce^{3+}$ energy transfer let us focus on the differences between the spectra obtained under excitation of $Tb^{3+}$ to the $^5D_3$ and $^5D_0$ states. One notices that the $Tb^{3+}$ contribution to the spectrum is stronger when the system is excited to the higher excited state $^5D_0$ than when it is excited to the $^5D_3$ state. This result is slightly confusing since one expects more effective $Tb^{3+}$ emission in the case of excitation with lower energy.

To understand this result one considers that the energy difference between the $^5D_3$ state and the $^7F_3$ state ($\widetilde{=}22\,200$ cm$^{-1}$) fits well (the energy differences between the $^5D_3$ state and the $^7F_2$, $^7F_1$ and $^7F_0$ fit even better) to the energy of the $Ce^{3+}$ excitation-band A. On the other hand, the energy of the $^5D_4$ state with respect to the ground state $^7F_6$ (20 490 cm$^{-1}$) is smaller than the energy necessary for excitation of the $Ce^{3+}$ ion through the f–d transition (the maximum of the $Ce^{3+}$ excitation band A corresponds to 21 740 cm$^{-1}$). Therefore, one can conclude that energy transfer between $Tb^{3+}$ and $Ce^{3+}$ takes place from the $^5D_3$ state before relaxation of $Tb^{3+}$ to the metastable $^5D_4$ state. In figure 4(b) the excited states of $Tb^{3+}$ labelled as 'sa' and 'sf' represent states of $5d^1 4f^7$. When the $Tb^{3+}$ is excited to $^5D_0$ the system can relax through nonradiative processes to the $^5D_3$, but also very probable is the nonradiative internal conversion from the $^5D_0$ to the state 'sf' of $5d^1 4f^7$. Then the system relaxes partly to the $^5D_3$ state and partly to the metastable $^5D_4$ state. The respective relaxation pathway is indicated by dashed arrows. On the other hand, when the system is excited into the $^5D_3$ state the energy barrier $E_{nr}$ prevents the nonradiative internal conversion between $^5D_3$ and the 'sf' state and therefore finally the occupation of the $^5D_4$ state is less probable. In this case, the alternative relaxation pathway from the $^5D_3$ state is nonradiative energy transfer to $Ce^{3+}$.

Pressure hardly changes the energy of the initial state $^5D_3$ of $Tb^{3+}$ and diminishes the energy of the final state $5d^1$ of $Ce^{3+}$. Since electron–lattice coupling causes the large vibronic broadening to the $Ce^{3+}$ absorption band, the pressure shift of $5d^1$ energy (for pressure below 100 kbar) does not influence strongly the energetic resonance and therefore does not influence the energy transfer process.

## 6. Conclusions

We have analysed the luminescence, luminescence excitation and dependence of the luminescence spectra on high hydrostatic pressure of cerium doped $(Y_{2.3-y}Ce_{0.05}Gd_y)Al_5O_{12}$ and $(Y_{2.3-x-y}Tb_xCe_{0.05}Gd_y)Al_5O_{12}$ for $y = 0.67$ and $x = 0.575$, 1.15, 1.725 and 2.3, respectively. We have estimated the pressure shift of the $5d^1 \rightarrow 4f^1$ luminescence of $Ce^{3+}$ ions and found that it is much larger than the respective shift of $Ce^{3+}$ emission in YAG. This effect has been tentatively attributed to the smaller bulk modulus of the $Y_{2.3-x}Tb_xCe_{0.05}Gd_{0.65}$ in comparison to the very hard YAG crystal. We have found that under excitation with wavelength 325 nm (approximately corresponding to $^7F_6 \rightarrow {}^5D_0$ transition in $Tb^{3+}$) we have $Tb^{3+}$ luminescence in all samples containing Tb. We have estimated the pressure dependence of the energies of the $^5D_4 \rightarrow {}^7F_6$, $^5D_4 \rightarrow {}^7F_5$, $^5D_4 \rightarrow {}^7F_4$ and $^5D_4 \rightarrow {}^7F_3$ transitions in $Tb^{3+}$.

We have analysed the mechanisms of $Tb^{3+}$ to $Ce^{3+}$ nonradiative energy transfer. We have found that such transfer takes place mainly from the $^5D_3$ excited state of $Tb^{3+}$. The efficiency of this transfer depends on $Tb^{3+}$ and does not depend on pressure up to 130 kbar.

Analysis of $Ce^{3+}$ excitation spectra in mixed crystals yields the conclusion that pressure and $Tb^{3+}$ content alter in different ways the $CeO_6$ complex. Pressure results in compression of the whole lattice and constantly compresses the $CeO_6$ complex, that results in an increase of

the crystal field. The increase of $Tb^{3+}$ content expands the lattice (increase of lattice constant) but simultaneously yields compression of the $CeO_6$ complex, that increases the crystal field.

## Acknowledgments

R S Liu would like to thank the Ministry of Economic Affairs of Taiwan for financial support under grant No 95-EC-17-A-07-S1-043 and the National Science Council of Taiwan for that under grant No 94-2113-M-002-030.

## References

[1] Kaminskii A A 1981 *Laser Crystals—Their Physics and Properties* ed H F Ivey (Berlin: Springer)
[2] Lin Y S, Liu R S and Cheng B-M 2005 *J. Electrochem. Soc.* **152** J41
[3] Lee S and Seo S Y 2002 *J. Electrochem. Soc.* **149** J85
[4] Grinberg M, Sikorska A and Kaczmarek S 2000 *J. Alloys Compounds* **300/301** 158
[5] Liu X and Ma L 1984 *Lumin. Disp. Dev.* **5** 93
[6] Inokuti M and Hirayama F 1965 *J. Chem. Phys.* **43** 1978
[7] Liu X, Wang X and Wang Z 1989 *Phys. Rev.* B **39** 10633
[8] Nakazawa E 1999 *Phosphor Handbook* ed W Shionoya and W M Yen (Boca Raton, FL: CRC Press)
[9] Barzowska J, Grinberg M and Tsuboi T 2003 *Radiat. Eff. Defects* **158** 39
[10] Shannon R D 1976 *Acta Crystallogr.* **751** A32
[11] Grinberg M, Barzowska J and Tsuboi T 2003 *Radiat. Eff. Defects* **158** 39
[12] Henderson B and Imbusch G F 1989 *Optical Spectroscopy of Inorganic Solids* (Oxford: Clarendon)
[13] Dorenbos P 2000 *J. Lumin.* **91** 155
[14] Dorenbos P 2000 *J. Lumin.* **91** 91
[15] Tröster Th, Gregorian T and Holzapfel W B 1993 *Phys. Rev.* B **48** 2960
[16] Gryk W, Dyl D, Ryba-Romanowski W and Grinberg M 2005 *J. Phys.: Condens. Matter* **17** 5381